18th Brazilian Congress of Thermal Sciences and Engineering
November 16-20, 2020 (Online)

ENC-2020-0551
DARRIEUS H-VAWT PERFORMANCE ANALYSIS USING FINITE VOLUME METHOD AND MULTIPLE STREAMTUBE

Larissa da Silva Pontes
Jakson Gomes de Oliveira Junior
PPGEM Master Student, Universidade Federal da Paraíba, João Pessoa/PB
larissa_pontes@outlook.com.br

João Alves de Lima
Renewable and Alternative Energy Center – DEER/CEAR/UFPB, Cid. Universitária, João Pessoa/PB
jalima@cear.ufpb.br

Abstract. *Wind energy has become a promising source of renewable energy. In particular, due to their low performance, vertical axis wind turbines (VAWT) are less used than horizontal axis wind turbines (HAWT). Nonetheless, they are suitable for unconventional installation areas, as they present lower variations in the power coefficient, lower noise emission and satisfactory reliability. In this work, the performance of an H-VAWT is evaluated using two approaches: the classical multiple streamtubes method (DART Code) and a computational fluid dynamic analysis (CFD) based on the finite volume method (ANSYS Fluent code). The former is used to obtain an initial rotor geometry that meets the power requirement for a given local wind condition and the last one is employed to verify this geometry. Numerical convergence was attained for time steps to which* $\Delta\theta \leq 1.8°$ *and meshes with divisions on the edges of the airfoil* $N_d \geq 300$*. For the DART code, the maximum power coefficient* $C_{pmax} = 0.29$ *was obtained for a tip speed ratio* $\lambda = 3.4$*, while with the Fluent code,* $C_{pmax} = 0.24$ *for* $\lambda = 3.0$*. The performance curves (*C_p *x* λ*) showed similar behavior, a negative power coefficient at low tip speed ratios (*$\lambda < 2.8$*) and a maximum power coefficient at similar tip speed ratios. The local power coefficient at the tip speed ration for maximum power coefficient (*$\lambda = 3.0$*) showed that in some regions it exceeds the Betz's limit, so this behavior is studied in the literature. The pressure gradient analysis showed why the power coefficient is negative for* $\lambda < 2.8$*, making the rotor unable to self-start.*

Keywords: *Wind Turbine, H-VAWT, Multiple Streamtubes, Finite Volume Method.*

1. INTRODUCTION

With the current environmental issues associated with the use of fossil fuels, the scientific community has turned its attention to the use of clean and renewable energy sources, such as wind power. Wind energy has been shown to be attractive for its abundance and for presenting low maintenance cost (Alaimo et al., 2015).

The mechanical element for transforming the kinetic energy from the winds into mechanical axis energy is called a wind turbine, and is normally classified into horizontal axis wind turbines (HAWT) and vertical axis wind turbines (VAWT), depending on the predominant wind direction in relation to its axis of rotation (Caser and Paiva, 2016).

According to Alaimo et al. (2015), although they seem conceptually out of date, the vertical-axis wind turbines proposed by Darrieus in 1931 are still of interest, due to some advantages over horizontal-axis turbines (Sumantraa et al., 2014): they do not need yaw mechanisms to align it in the direction of the wind so that they can operate and are suitable for small scale energy production. With these characteristics, these turbines can be installed in urban areas, where the direction and magnitude of the wind vary widely due to the presence of barriers such as buildings and other structures that interfere in the passage of the wind. Furthermore, these turbines operate at relatively low speeds, which makes them produce less noise.

In general, the performance of wind turbines can be estimated analytically, numerically and experimentally. As in any analysis, the analytical form of analysis is limited to a few simple situations, so that the numerical methods (simple or advanced) and experimental are the most used today. According to Alaimo et al. (2015) the simplest numerical models currently used are models based on the blade element theory (such as multiple streamtubes), those based on the vortex representation of the blades and their wake and the cascade models.

The momentum models are based on the relation between the change in the momentum of the air through the rotor and the drag force. These models can predict the performance curve of a rotor with an acceptable level of accuracy (Strickland, 1975). According to Islam et al. (2008) there are three momentum-based models: single streamtube, multiple

streamtube and double multiple streamtube. The first one assumes a single streamtube that encloses the whole rotor and tends to overestimate the power coefficient of the rotor.

The multiple stramtubes model is an improvement to the single streamtube model. Here, the volume of the rotor is divided into a series of parallel streamtubes and then the blade element and momentum theories are applied to each streamtube. This model shows better accuracy than the single streamtube, but still tends to overestimate the power coefficient (Islam et al., 2008).

According to Islam et al. (2008), the double multiple streamtubes model is based on the multiple streamtubes one, but the calculation is done for the upstream and downstream portion of the rotor separately. It can give better results than the other two, but still can overpredict the overall performance of the turbine and may have convergence problems.

Of these models, the vortex model is considered the most accurate, but it has the highest computational cost and, in some situations, it has convergence problems. On the other hand, the multiple streamtubes requires less computational capacity, but the model does not respond well in high wing tip speed ratios and high solidity. The cascade model supports high wing tip speed ratios and high solidity (Alaimo et al., 2015).

Another numerical method for the analysis of the aerodynamic properties of VAWTs is the finite volume method. The URANS equations (unsteady Reynolds-averaged Navier-Stokes) allow the study of phenomena that the previous models cannot analyze, such as, for example, the aerodynamic stall that occurs at low wing tip speed ratios (Rogowski, 2019). Balduzzi et al. (2016) evaluated the performance of three turbulence models in the analysis of Darrieus rotors, namely: Standard k-ε, RNG k-ε and SST k-ω. His work showed that VAWT analysis is best performed using the SST k-ω model, due to its improved ability to evaluate adverse pressure gradients from fluid separation and free flow, showing better stability and agreement with experiments.

2. METHODS

The rotor to be analyzed has its characteristics presented in Tab. 1. This rotor, a scale model based on similarity analysis and on a series of historical wind data for the city of João Pessoa-PB, will be designed to operate at a free flow speed in a wind tunnel V_∞ = 15.89 m/s, with an output power of 25 W.

The present work seeks to study this rotor without the influence of its structure (connecting elements and shaft), comparing the results obtained with the simplified model of multiple stream tubes with those obtained via a two-dimensional model based on computational fluid dynamics (CFD), which uses the finite volume method and the k-ω SST turbulent model, in order to determine its power coefficient curve (C_p) versus wing tip speed ratio (λ).

Table 1. Main characteristics of the rotor

Airfoil	NACA 0025
Aspect Ratio	2
Solidicity	0.45
Number of blades	3
Radius (cm)	15.9
Height (cm)	31.8
Chord (mm)	23.9
Rotational Velocity (RPM)	3,243.8

The DART code (DArrieus Rotor Turbine), developed by Strickland (1975) and which is based on the multiple streamtubes model, was used to perform simplified analyzes of the rotor. This code requires as input data the aspect ratio of the turbine (HR), the number of blades (N), the solidity (σ) and the Reynolds number (Re) (to obtain the aerodynamic coefficients of the blade airfoil, Sheldahl and Klimas, 1981). From the DART code calculations associated to the optimization procedure by Brusca et al. (2014), it is possible to obtain a rotor geometry (radius, R and profile chord, c) that operates at determined rotation speed, in addition to evaluate its power coefficient (C_p) versus ratio of wing tip speed (λ). By varying the rotor solidicity, it is possible to obtain a geometry that presents the maximum power coefficient for the pre-established wind conditions (V_∞) and required power output (Brusca et al., 2014).

The previous methodology offers a first estimate of the dimensions of a turbine's rotor using a simplified approach, although very useful, does not take into account several important factors. Thus, the CFD Fluent code (ANSYS, 2013) is used to perform a two-dimensional analysis. Despite being two-dimensional, this methodology incorporates most of the effects that are not taken into account in the previous methodology such as the effects of the wake on the blades in the region posterior to the center of the rotor, the dynamic stall and the effects of flow curvature (Balduzzi et al., 2016). Balduzzi et al. (2016) also states that for some applications, the 2D method can also be used successfully to estimate the performance of the rotor. Three-dimensional analyzes are used only when a higher level of precision is desired in the estimation of the power coefficient, where some effects that are not analyzed in the 2D model must be computed.

The study begins with determining the size of the domain in order to minimize its influence on the flow around the rotor. The dimensions of the domain adopted in the present work were based on the work developed by Bianchini et al.

(2015) and are shown in Fig. 1, where *D* is the diameter of the rotor (taken as the characteristic length scale). The domain was divided into two parts, a static and a dynamic one (where the rotor is inserted and which has a 2D dimension). For modeling turbulence, Balduzzi et al. (2016) recommends the k-ω SST model and the sliding mesh technique to simulate the flow in VAWTs. This approach was used in the present work. The SIMPLEC algorithm was used to solve the pressure-velocity coupling and a second order upwind scheme was applied to the spatial discretization of momentum, energy and turbulence. A second order implicit formulation was used in the transient terms.

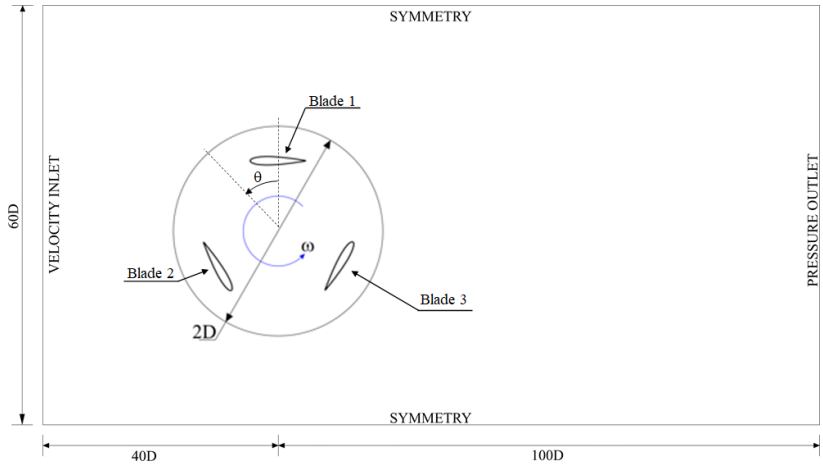

Figure 1. Domain dimensions.

The air (that flow through the domain) proprieties were set to the standard values present in the Fluent's material database. The boundary conditions were defined as Velocity Inlet at the inlet of the flow with a velocity magnitude of 15.89 m/s normal to the boundary. At the outlet of the flow, a Pressure Outlet condition was defined with a gauge pressure equal to 0 Pa. A Symmetry condition was applied on the sides of the domain as recommended by Bianchini et al. (2015). Turbulence intensity and viscosity ratio were set to the Fluent default values (5% and 10, respectively) in all boundaries.

The circular region in which the blades are inserted is a rotating domain with the same angular velocity as the blades (ω = 3243.8 RPM). For the rotating subdomain to be able to rotate, two distinct meshes must be created for each of the subdomains, so that an Interface condition must be defined. In the present work, the standard interface condition was used. On the blade surfaces, a Moving wall condition with zero angular velocity relative to the circular subdomain was imposed.

The mesh generation was performed using ANSYS Meshing. An unstructured mesh was created for each subdomain separately, but with care so that the interface nodes between the two subdomains coincide. The Inflation tool was applied to the airfoil surface and the thickness of the first layer (ΔS) was calculated to satisfy $y^+ \approx 1$. A total of 40 layers with a Growth Rate of 1.1 was imposed on Inflation. In the region of the rotating sub-domain where the blades circulate, a finer mesh was applied where the pressure and speed gradients are more marked (Lanzafame et al., 2014). Figure 2 shows a mesh overview.

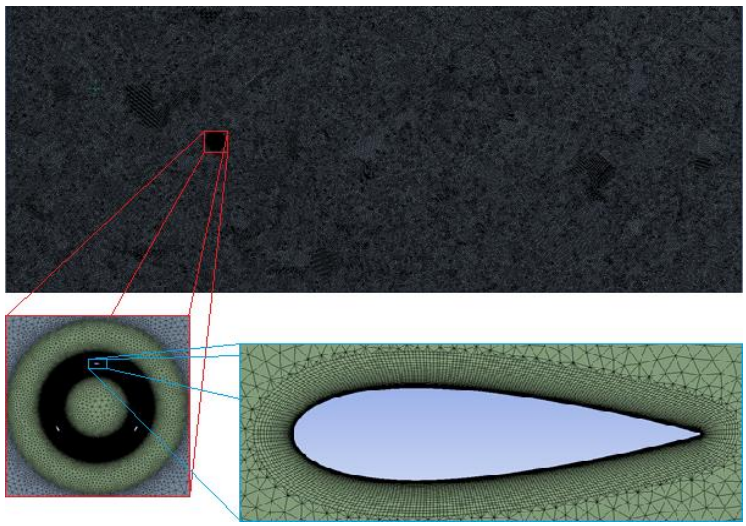

Figure 2. Mesh details.

Mesh convergence and time step size studies were carried out that satisfied a tolerance of 10^{-5} for all calculation variables (mass, momentum, pressure and turbulence variables) and 100 iterations per time step. The mesh convergence study was performed considering only the variation in the number of divisions on the blade airfoil surface (Alsabri et al., 2019). The following values for the number of divisions N_d of the profile were considered: 200, 250, 300, 350 and 400.

The time step was evaluated considering an angular variation of the rotor ($\Delta\theta$) that corresponds to the time necessary for the rotor to advance a certain portion of the complete turn around its axis. For the analyzed rotation (3,243.8 RPM), the following values of $\Delta\theta$ were considered in the analyzes: 2%, 1%, 0.5%, 0.2% and 0.1% of time of a complete rotation, which correspond to the following angular variations: 7.2º, 3.6º, 1.8º, 0.72º and 0.36º, respectively.

Due to the high time required to verify the number of complete revolutions necessary for achieve convergence of the power coefficient, the authors chose not to carry out this study. However, Rogowski (2019) demonstrated in his work that only 10 complete rotations would be necessary to observe the convergence of the power coefficient of the Darrieus H-rotor that he studied; this was the number adopted in this work to consider the convergence of the power coefficient.

3. RESULTS

Figure 3 shows the evolution of the convergence of the power coefficient with the decrease in the size of the time step (for the mesh with 150 divisions in the blade airfoil). From this figure, it can be seen that, for an angular discretization $\Delta\theta$ less than or equal to 0.5% (1.8 degrees), it can already be considered that the power coefficient (C_p) is converged. The convergence of C_p (approximately 0.23) with greater angular discretization is due to better accuracy in capturing data from the wake where one blade crosses the wake of another.

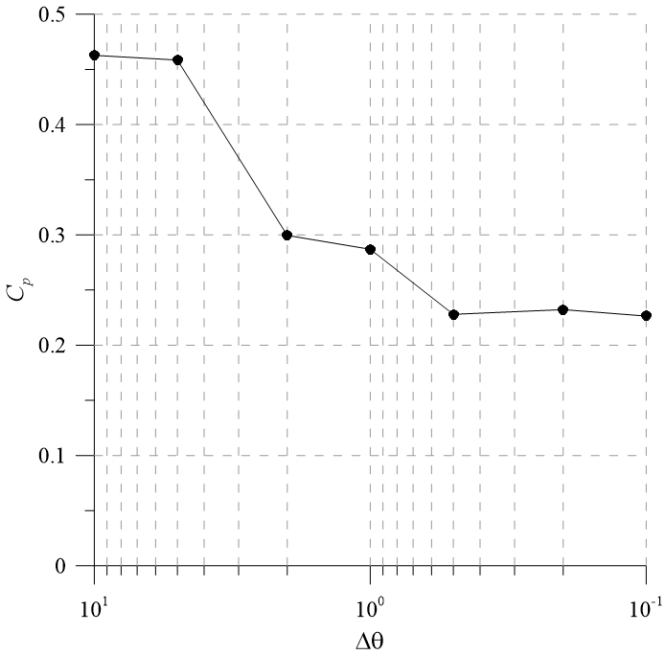

Figure 3. Power coefficient convergence (C_p) versus time discretization in percentual ($\Delta\theta$).

The spatial mesh convergence test is now performed based on the behavior of the previous temporal discretization. For this analysis, $\Delta\theta$ = 0.5% (1.8 degrees) was considered.

Figure 4 shows the variation of the rotor power coefficient with the number of mesh divisions N_d in the blade airfoil. The figure shows that the rotor power coefficient reaches convergence with a number of divisions greater than or equal to 300, which is the number considered for the following analyzes. A slight increase in C_p can be seen in the figure with an increase in the number of divisions in the blade airfoil.

The performance curves (C_p versus λ) of the rotor obtained with the DART code and with the two-dimensional CFD analysis in Fluent are compared in Figure 5. There is a difference between the results obtained with the two methods used. This difference is mainly due to the fact that the simulations in Fluent consider a series of effects that DART does not compute, which leads to a difference in the power coefficient when comparing the results. However, both analyzes reproduced the same behavior of the curve. The maximum power coefficient estimated by Fluent is 0.24 for λ = 3 and by DART is 0.29 for λ = 3.4.

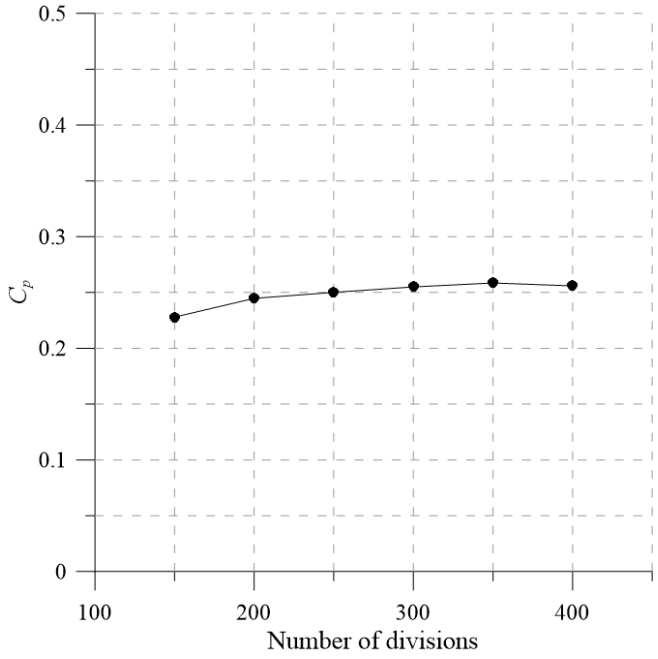

Figure 4. Power coefficient convergence (C_p) versus number of divisions in airfoil edge.

The curves show one of the main characteristics of a Darrieus rotor: the difficulty in performing the self-start. For this particular geometry, it is impossible for the rotor to start alone from rest as there are negative values of power coefficient for lower values of wing tip speed ratio (λ).

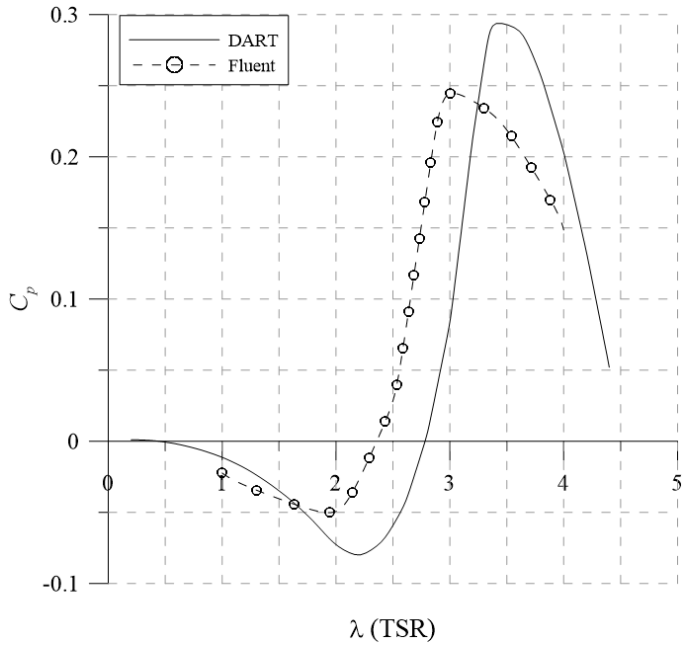

Figure 5. Average power coefficient (C_p) versus tip speed ratio (λ) for the two numerical methods.

Figure 6 shows the torque coefficient for each blade over a complete rotation for λ = 3 and 2. These values represent the tip speed ratios that corresponds to the higher and lower power coefficients, according to Fig. 5.

From Fig. 6a (λ = 3), it can be seen that the blade 1 provides a maximum torque (C_t = 0.43) at θ = 88,2º and a second peak at θ = 216º (C_t = 0.17). There are two regions where C_t is negative, but in most of the angular position the torque coefficient contributes to the generation of energy. The same behavior is observed for the two other blades, shifted 120º for blade 2 and 240º for blade 3. From Fig. 6b, it is possible to see that in most of the rotation, the blades produce a negative torque coefficient resulting in a negative power coefficient as seen in Fig. 5.

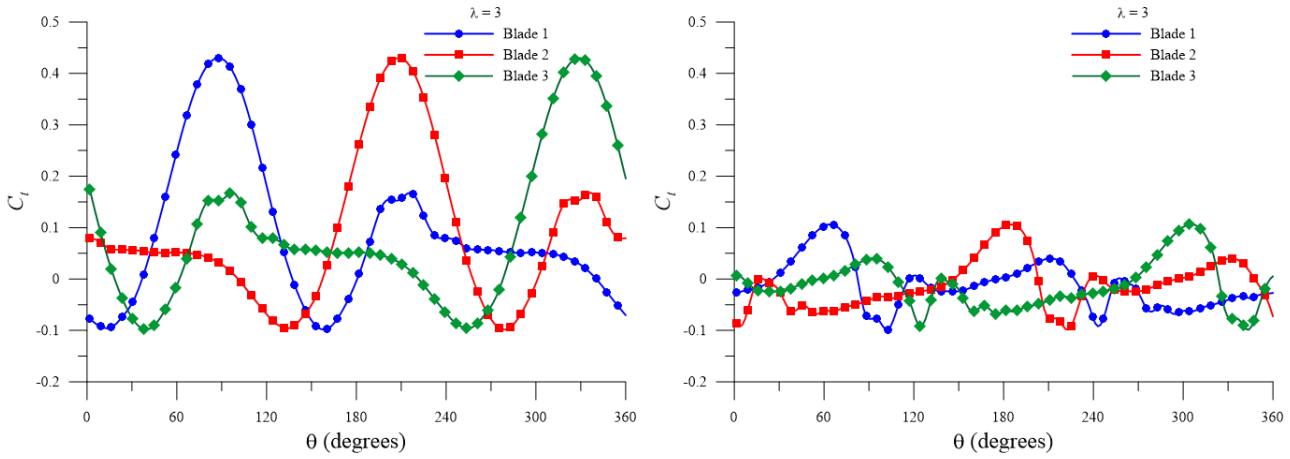

Figure 6. Torque coefficient (C_t) versus azimuthal angle (θ) for each blade for (a) λ = 3, (b) λ = 2.

The instantaneous power coefficient (C_p x θ) of the rotor over a complete rotation is shown in polar form in Fig. 7 for the two extreme tip speed ratios, λ = 3 and λ = 2.

As observed in Fig. 7a (λ = 3), there are three peaks of power coefficient out of phase 120º from each other that correspond to the maximum contribution point of each blade. The performance curve of one of the blades can also be seen in the same figure. It can be seen that the maximum performance of the blade 1 is aligned to one of the peak power coefficients of the rotor.

Fig. 7b shows the behavior of the instantaneous power coefficient for λ = 2 (tip speed ratio for minimum power coefficient). It can be noticed an irregular behavior for both blade and rotor and a negative power coefficient at most of the rotation agreeing with Fig. 5 at λ = 2. This phenomenon reiterates observation that this rotor is incapable of generate power for low tip speed ratios.

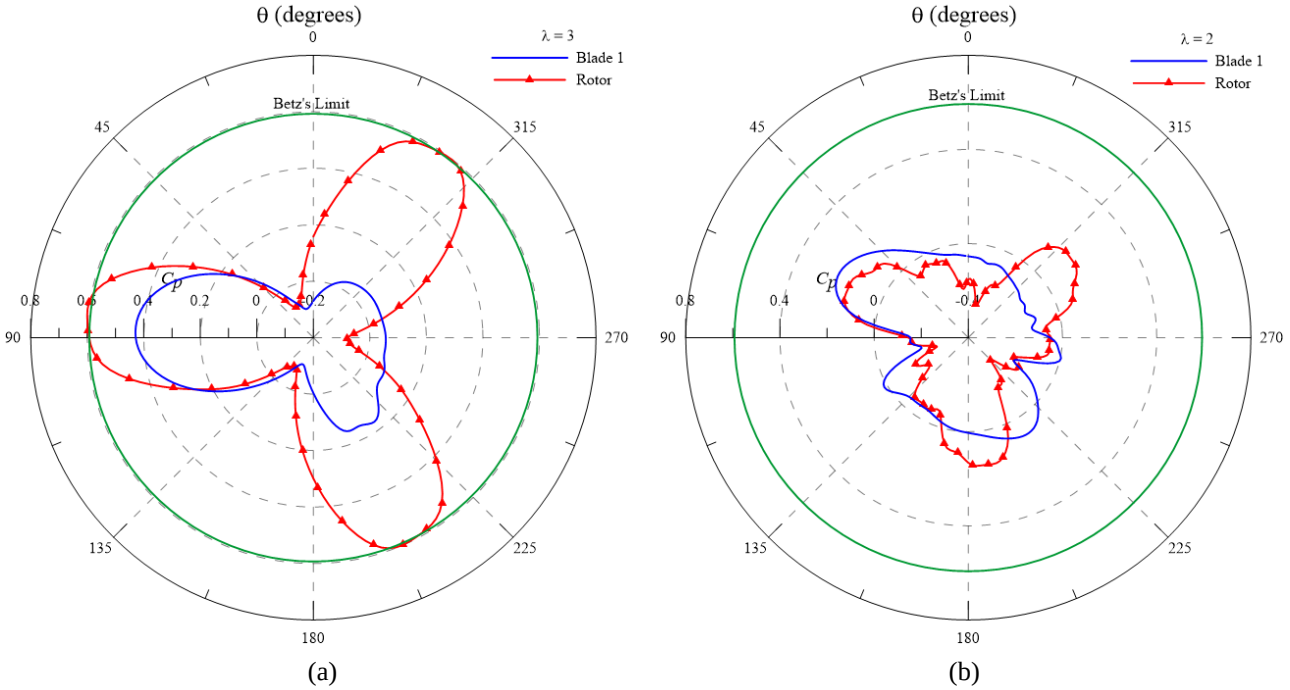

Figure 7. Power coefficient (C_p) versus azimuthal angle (θ) for blade 1 and entire rotor for (a) λ = 3, (b) λ = 2.

From Fig. 7a, it can be seen that the local maximum power coefficient goes above Betz's limit, reaching a maximum of 0,61. According to Castelli et al. (2011), this behavior can be related to the sudden pressure drop around the rotor region, especially for maximum local azimuthal position. To better illustrate this relation, Fig. 8 shows a 3D representation of the pressure contour for azimuthal position of maximum local C_p(θ) (blade 1 at 82,8º) and λ = 3.

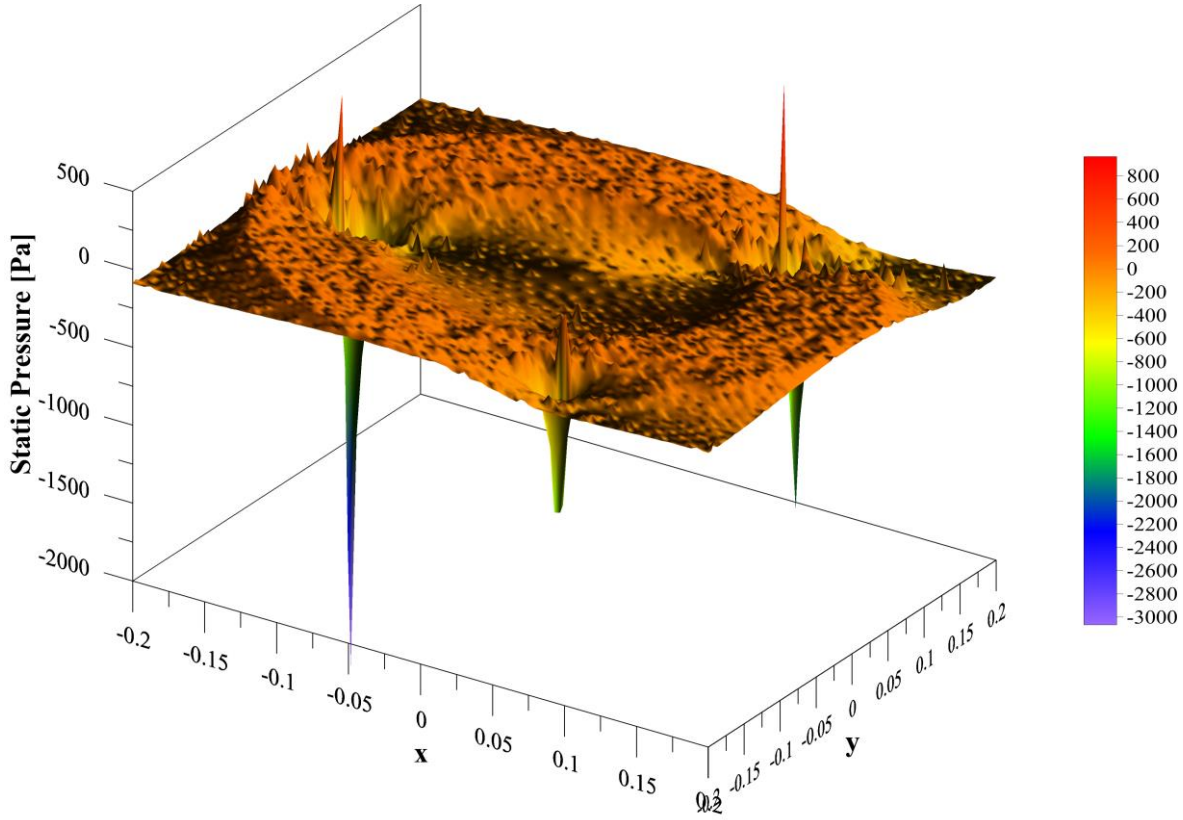

Figure 8. 3D representation of the pressure contour for θ = 82.8º (Cp_{max}) and λ = 3.

In the words of Castelli et al. (2011), "this phenomenon could be considered the main responsible for the local increase of the instantaneous power coefficient and should be further investigated".

General pressure contours around the blades for azimuth angles (θ) of 0º, 120º and 240º can be seen in Fig. 9 for λ = 3. It can be noticed that there is a small zone of high pressure in the leading edge of the blade that starts to reduce its value and move as the blade rotates, as shown in the following angles (120º and 240º). There is also a region of negative pressure close to the leading edge of the profile that also changes position as the blade rotates. According to Feng *et al.* (2018), this pressure difference drives the blade forward.

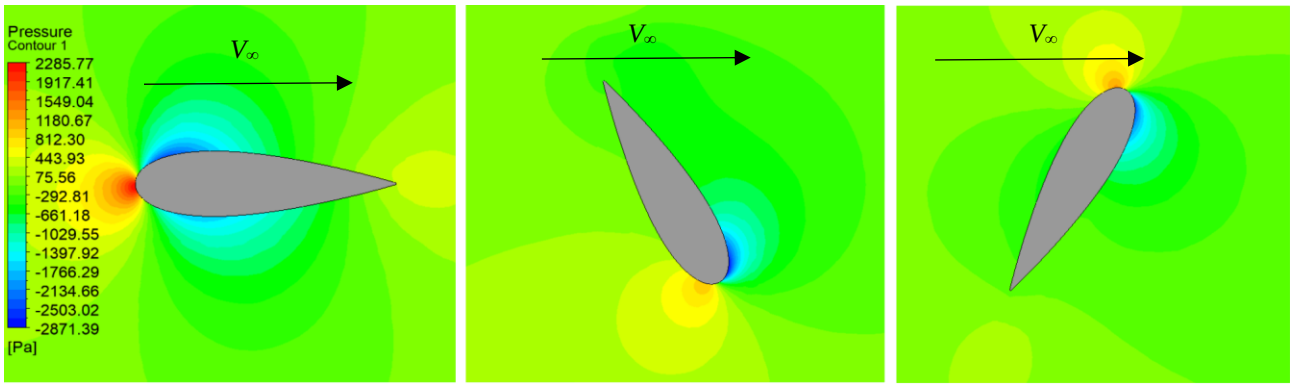

a) θ = 0° b) θ = 120° c) θ = 240°

Figure 9. Pressure contour around the blade for three different blade positions.

Figures 10 and 11 show the pressure contour for λ = 3 at the blade positions for maximum and minimum local power coefficient, respectively. It can be noticed in Fig. 11, as it would be expected, a lower pressure gradient near the blades when compared with Fig. 10. This leads to lower local torque coefficient and power coefficient once pressure gradients are the responsible to drive the blade forward. A comparison between Fig. 10 and 11 reveals why higher local power coefficients are obtained in the first situation: higher pressure gradients are observed at the ventral section of the blades in Fig. 10.

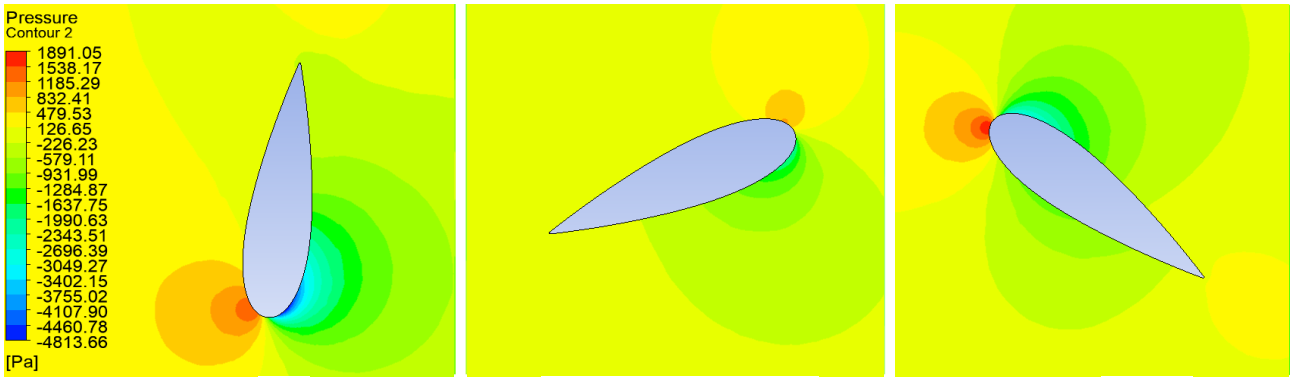

a) θ = 82.2° b) θ = 202.2° c) θ = 322.2°

Figure 10. Pressure contour around the blade for three different blades for the maximum power coefficients positions.

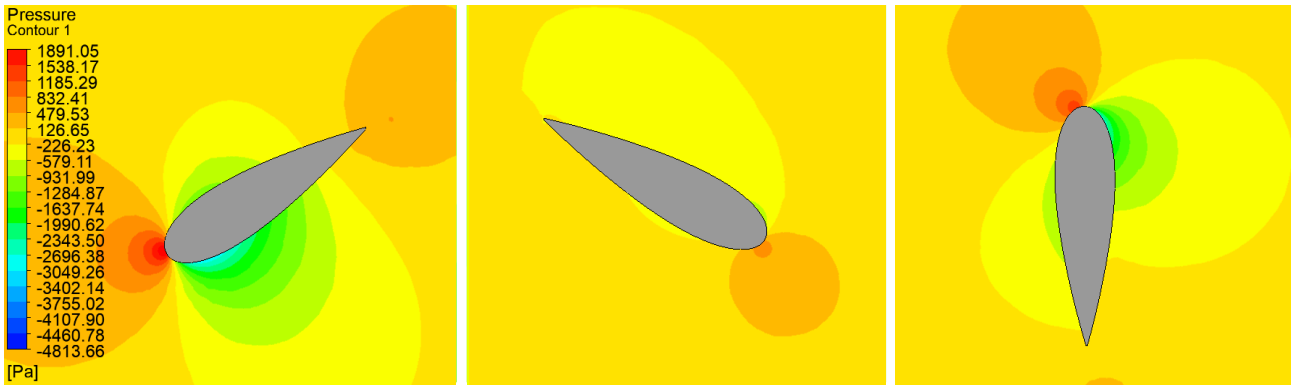

a) θ = 27.0° b) θ = 147.0° c) θ = 267.0°

Figure 11. Pressure contour around the blade for three different blades for the minimum power coefficients positions.

Figure 12a illustrates the velocity contour and streamlines around the rotor and Fig. 12b shows the related vorticity field. From Fig. 12a, it is possible to see the influence of the rotor at the windward side showing that the streamlines are curving as they get close to the rotor. It is evident the capacity of the model in predicting the stall and wake effects. Furthermore, the distortion observed in the streamlines along the blades trajectories is due to the vorticity created by the rotor rotation as can be seen in Fig. 12b. It can also be noticed the influence of one blade wake on the flow of the subsequent one.

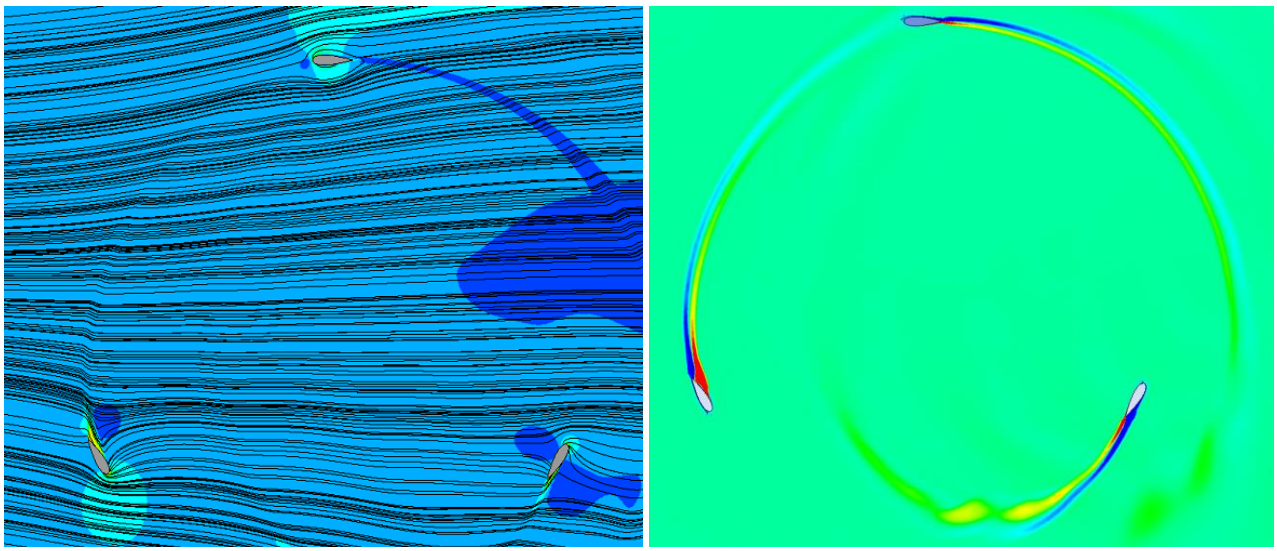

(a) (b)

Figure 12. a) Velocity contour and streamlines around the rotor, b) Vorticity field.

Figure 13 shows zooms of the velocity contours and the streamlines for the same three blade positions for λ = 3 depicted in Fig. 12. At θ = 0º, smoother streamlines are observed as the induced angle of attack is close to zero. For θ equal to 120º and 240º, more curved streamlines are displayed because in these angular positions higher angle of attack, close to the aerodynamic stall, are present.

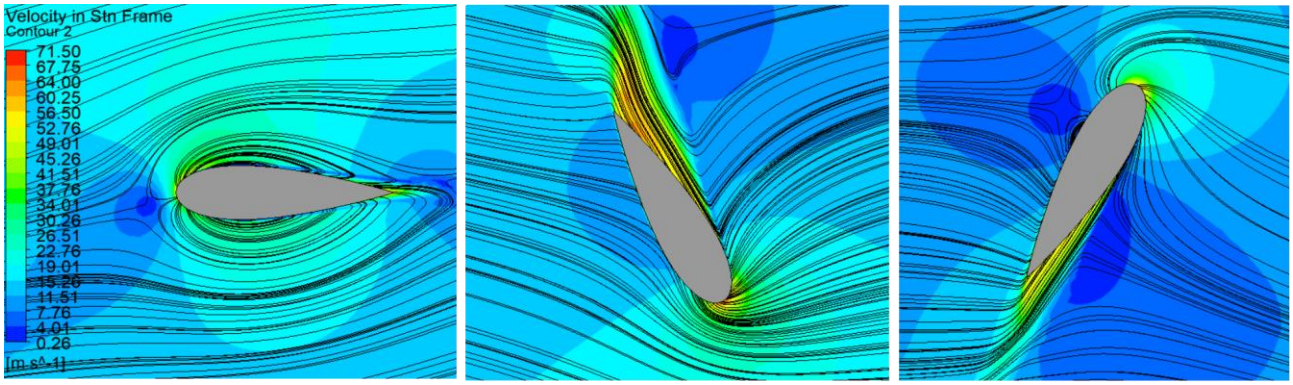

a) θ = 0° b) θ = 120° c) θ = 240°

Figure 13. Velocity contour and streamlines around the blade for three different blade positions.

4. CONCLUSIONS

This work was sought to analyze the performance of a VAWT using two different numerical models, starting from the rotor geometry and the operating conditions. The multiple-streamtube model was used to study the general performance of the rotor as it is a simple and fast convergence approach. In association with the DART code (based on the multiple-streamtube model), the optimization methodology proposed by Brusca et al. (2014) and a similarity analysis were employed to obtain a geometry (and the operational rotation) that is, possibly, the most efficient for a given wind and power requirement.

The finite volume method was then used to evaluate the performance of the rotor considering the aerodynamic effects that multiple-streamtube approach do not take into account, despite being a more complex and high computational cost method. Although a three-dimensional model is more accurate and thus indicated in analyzing the efficiency of the rotor, a two-dimensional model was used because it is able to predict, with a good level of accuracy, the overall and detailed performance of the rotor.

When comparing both methods, it was possible to estimate a maximum power coefficient C_{pmax} = 0.29 using DART code and a C_{pmax} = 0.24 using Fluent. Both models showed the same behavior for the performance curves (C_p x λ), a negative power coefficient at low tip speed ratios (λ < 2.8) and a maximum power coefficient at similar tip speed ratios. It was showed that each blade passes through zones where they produce a negative torque coefficient, but the overall torque coefficient contributes to power generation.

The local torque coefficient and local power coefficient were showed for the tip speed ratios that correspond to the lowest and highest power coefficient (λ = 2 and λ = 3, respectively). For λ = 3, it can be noticed that the local power coefficient exceeds the Betz's limit for some azimuthal positions and can be related to the sudden pressure drop around the rotor region as explained by Castelli et al. (2011).

Pressure contours were showed for nine different blade azimuthal positions, including those for maximum and minimum local power coefficient. It was evidenced the differences of the pressure gradient at these regions that drives the blades forward.

Finally, as a continuation of the work, it is proposed to perform three-dimensional simulations and rotor tests in a wind tunnel for comparison with the models presented here. The experimental results will serve as a basis for the validation of the computational models presented.

5. REFERENCES

ALAIMO, Andrea et al. 3D CFD Analysis of a Vertical Axis Wind Turbine. *Energies*, [S.L.], v. 8, n. 4, p. 3013-3033, 17 abr. 2015. MDPI AG.

ALSABRI, Ahmad; OREIJAH, Mowffaq; MOHAMED, M. H.; MAKKAH. A Comparison Study of Airfoils Used in H - Rotor Darrieus Wind Turbine. *International Journal Of Science And Engineering Investigations*, [S.L.], v. 8, n. 90, p. 22-28, 2019.

BALDUZZI, Francesco; BIANCHINI, Alessandro; MALECI, Riccardo; FERRARA, Giovanni; FERRARI, Lorenzo. Critical issues in the CFD simulation of Darrieus wind turbines. *Renewable Energy*, [S.L.], v. 85, p. 419-435, jan. 2016.

BIANCHINI, Alessandro; BALDUZZI, Francesco; RAINBIRD, John M.; PEIRO, Joaquim; GRAHAM, J. Michael R.; FERRARA, Giovanni; FERRARI, Lorenzo. An Experimental and Numerical Assessment of Airfoil Polars for Use in Darrieus Wind Turbines—Part II: post-stall data extrapolation methods. *Journal Of Engineering For Gas Turbines And Power*, [S.L.], v. 138, n. 3, p. 1-10, 22 set. 2015. ASME International.

BRUSCA, S.; LANZAFAME, R.; MESSINA, M.. Design of a vertical-axis wind turbine: how the aspect ratio affects the turbine′s performance. *International Journal Of Energy And Environmental Engineering*, [S.L.], v. 5, n. 4, p. 333-340, 2 ago. 2014.

CASER, Eduardo Spalenza; PAIVA, Giuseppe da Mota. *Projeto aerodinâmico de uma turbina eólica de eixo vertical (TEEV) para ambientes urbanos*. 2016. 71 f. TCC (Graduação) - Curso de Engenharia Mecânica, Departamento de Engenharia Mecânica, Universidade Federal do Espírito Santo, Vitória, 2016.

CASTELLI, Marco Raciti; ENGLARO, Alessandro; BENINI, Ernesto. The Darrieus wind turbine: proposal for a new performance prediction model based on cfd. *Energy*, [S.L.], v. 36, n. 8, p. 4919-4934, ago. 2011.

FENG, Fang; ZHAO, Shouyang; QU, Chunming; BAI, Yuedi; ZHANG, Yuliang; LI, Yan. Research on Aerodynamic Characteristics of Straight-Bladed Vertical Axis Wind Turbine with S Series Airfoils. *International Journal Of Rotating Machinery*, [S.L.], v. 2018, p. 1-13, 2018. Hindawi Limited

FLUENT Manual - ANSYS Release Version 15.0, *Theory Guide*; ANSYS Inc.: Canonsburg, PA, USA, 2013.

ISLAM, Mazharul; TING, David S. K; FARTAJ, Amir. Aerodynamic models for Darrieus-type straight-bladed vertical axis wind turbines. ***Renewable And Sustainable Energy Review*s**, [S.L.], v. 12, n. 4, p. 1087-1109, 2008. Elsevier.

LANZAFAME, Rosario; MAURO, Stefano; MESSINA, Michele. 2D CFD Modeling of H-Darrieus Wind Turbines Using a Transition Turbulence Model. Energy Procedia, [S.L.], v. 45, p. 131-140, 2014.

R., Bose Sumantraa; S., Chandramouli; P., Premsai T.; P., Prithviraj; M., Vivek; KISHORE, V. Ratna. Numerical Analysis of Effect of Pitch Angle on a Small Scale Vertical Axis Wind Turbine. *International Journal Of Renewable Energy Research*, [S. L.], v. 4, n. 4, p. 929-935, 06 nov. 2014.

ROGOWSKI, Krzysztof. CFD Computation of the H-Darrieus Wind Turbine—The Impact of the Rotating Shaft on the Rotor Performance. *Energies*, [S.L.], v. 12, n. 13, p. 2506-2524, 28 jun. 2019. MDPI AG

SHELDAHL, Robert E.; KLIMAS, Paul C.. *Aerodynamic Characteristics of Seven Symmetrical Airfoil Sections Through 180-Degree Angle of Attack for Use in Aerodynamic Analysis of Vertical Axis Wind Turbines*. Albuquerque: Sandia Laboratories, 1981. 124 p.

STRICKLAND, James H. The Darrieus Turbine: *A Performance Prediction Model Using Multiple Streamtubes*. Albuquerque: Sandia Laboratories, 1975. 37 p.

6. RESPONSIBILITY NOTICE

The authors are the only responsible for the printed material included in this paper.